# Computational measurement of void percolation thresholds of oblate particles and thin plate composites

Y. B. Yi[a] and K. Esmail
*Department of Mechanical and Materials Engineering, University of Denver, Denver, Colorado 80208, USA*

The void percolation thresholds of random oblate particles and thin plate composites are measured computationally using the lattice mapping technique and the Monte Carlo simulation scheme. Two types of spatially uncorrelated inclusions have been investigated: oblate ellipsoids and elliptical thin plates, with which the site and bond percolation systems are developed separately. The results are obtained from the finite-size lattices followed by a mathematical extrapolation to the infinite domains. The computational results are validated by a comparison with the numerical solutions of the limiting cases found in the literature. It is concluded that the void percolation thresholds of oblate inclusions have a much stronger dependence on the geometric aspect ratio of the inclusions compared to those of the prolate counterparts. In the limit, the percolation threshold $\eta$ is measured to be 22.86 for circular thin disks. Approximate solutions are presented in the form of polynomial functions and Pade approximants. The results have potential applications in composite material designs and molecular diffusion problems. © 2012 American Institute of Physics. [http://dx.doi.org/10.1063/1.4730333]

## I. INTRODUCTION

Percolation is a phenomenon where one or more domain-spanning pathways exist in a physical system.[1] Measurement of the geometric percolation threshold, i.e., the minimum amount of the material phase required for percolation, is typically one of the fundamental tasks in design and optimization of advanced heterogeneous materials for better performances.[2,3] Over the past decades, the percolation phenomena have been studied via the developments of a variety of analytical and computational schemes.[4] The measurements of percolation thresholds in both two-dimensional[5,6] and three-dimensional systems[7] have been well documented, but the quantitative determinations of the morphological effects on noncircular or nonspherical particles were not attempted until very recent,[8,9] partly due to the intensive computation involved in both analytical and numerical approaches.

It is well known that percolation can occur in either the material phase or the void space in a composite material system. In the latter case, the percolation is called a *void percolation* or *Swiss-cheese percolation*,[10] namely, in a cheese-like continuum where particles are cut away, the percolation through the cheese itself is considered. One of the earliest applications of void percolation is in fluid mechanics when fluids flow through porous structures. Recently, molecular or atomistic diffusion in heterogeneous structures, such as gas diffusion in battery electrolytes[11] and intracellular ion transport in cytoplasm,[12] aroused new interest in void percolation problems. This is because the diffusion processes in these materials often occur at small scales and have irregular pathways formed by the void space in the material microstructures. However, it is not clear at present how to effectively model the dynamic motions of molecules through a confined pathway. There exist several distinct tools for simulating diffusion processes, including continuum diffusion, molecular dynamics,[13] and random walk simulations.[14] However, it is unknown how the existence of the voids may affect the molecular motions and thus the equivalent coefficient of diffusion. To answer this question, it is essential to understand how the structural morphology alters the local and global probabilities of void percolation.

Despite the complexity in the mathematical treatment and the considerable amount of computational effort involved in void percolation studies, there was significant progress in this area. For example, it has been known that the void percolation for monodisperse systems can be simplified by mapping the system to a bond network associated with the Voronoi tessellation of the sphere centers.[15] Recently, some efficient techniques were also developed by implementing the scaling theories[16] and growth algorithms[17] to obtain very precise results for void percolation thresholds of monodisperse sphere systems.

Realistic particulate materials, however, do not possess idealized spherical or circular shapes. It is interesting to know whether the aspect ratio of the particulate inclusions has any significant effect on the void percolation threshold. Recently, it was confirmed that there are no universalities for void percolation threshold of ellipsoidal particles and that void percolation associated with inclusions of large aspect ratio should be treated differently from that of spheres.[18] However, this work was based on the prolate geometries, while the particles in many applications involve oblate geometries. For example, macromolecular diffusion in cells can be modeled by considering the available space in cytoskeletal networks and internal membranes in cells.[19] This was achieved by approximating intracellular structures as mixtures of random overlapping obstacles of various prolate or oblate shapes. In particular, the cytoskeletal filaments were modeled as long thin cylinders

[a]Author to whom correspondence should be addressed. Electronic mail: yyi2@du.edu.

whereas *endoplasmic reticulum* structures were represented by thin disks.[20] The shapes of the intracellular environment have been shown to bring about a four-to-fivefold reduction in diffusive transport, compared to diffusion in cytosol free of intracellular structures.

Since the ionic diffusion problems are closely related to void percolation, it is interesting to know whether the same conclusions drawn from the past research can apply to oblate systems as well. In particular, one may ask: does the void percolation threshold of an oblate system have the same aspect ratio dependence as a prolate system?

Modeling void percolation of ellipsoids is more computationally intensive due to the increased degrees of freedom in each particle. Although the Voronoi tessellation equivalence does not apply to ellipsoidal particles, by mapping the void continuum system into its lattice equivalent, it is possible to employ the Monte Carlo schemes to measure the percolation properties. This in fact was already accomplished in the author's prior research on prolate ellipsoidal systems[18] and is equally applicable to oblate systems as well. In addition, when one of the axes of an oblate ellipsoid approaches zero, the geometry will degenerate to an elliptical plate. By refining the equivalent lattice system with a sufficiently large number of sites or bonds, the asymptotic solutions can be obtained from mathematical extrapolations.

## II. METHODS

### A. Lattice mapping technique

A lattice mapping technique was employed to formulate the void percolation system of interest. It was followed by an efficient computational algorithm for finding the existence of any percolation path. More specifically, a three-dimensional unit cell was divided into $p \times p \times p$ points, where $p$ represents the number of points on each side. These points are denoted as *sites* and the connections between two neighboring sites are denoted as *bonds*. Oblate ellipsoids or elliptical plates were then generated randomly inside the cell following a standard Poisson process. For oblate ellipsoids, they were uncorrelated, equisized particles of revolution with the aspect ratio, $\varepsilon$ being defined as the radius of revolution, $r$ divided by the half thickness, $t$. For elliptical plates, $\varepsilon$ is defined as the ratio of the major axis length, $a$, to the minor axis length, $b$. Therefore, in both cases we have $\varepsilon \geq 1$.

For oblate ellipsoids, a site percolation problem was formulated, i.e., the locations of the sites relative to each ellipsoidal surface were examined. Those sites in the interior of at least one ellipsoid were labeled as "absent," whereas the remaining sites were labeled as "present." The present sites were therefore a collection of those sites in the void space of the system, and the percolation path was sought for those sites accordingly. The lattice system was binned based on the locations and sizes of the ellipsoids. Only those sites located inside the "bin" were examined for their coordinates relative to the ellipsoid. For a site whose position vector is r, and an ellipsoid specified by the location $\mathbf{r}_0$ of its center, as well as the orientation angle $\omega$ in space, we define a *contact function F* (Ref. [21]) whose value $< 1$ for **r** inside the

ellipsoid A; $F = 1$ for **r** located on the surface of A; and $F > 1$ for **r** outside A

$$F(\mathbf{r} - \mathbf{r}_0, \omega) = (\mathbf{r} - \mathbf{r}_0)^T A^{-1} (\mathbf{r} - \mathbf{r}_0), \qquad (1)$$

wherein $T$ indicates the transpose operator, and

$$A(\omega) = \sum_{i=1}^{3} R_i(\omega) R_i^T(\omega), \qquad (2)$$

where $R_i$ $(i = 1, 2, 3)$ are the vectors comprising the semiaxes.

For elliptical thin plates, however, a site percolation formulation would be inappropriate since a plate has zero volume and there would be no sites encompassed by any plate. The percolation problem was therefore formulated as a bond percolation system instead. The location of each bond, i.e., the line segment in the lattice system, was compared to the elliptical surface equations. An intersection between a bond and an elliptical surface would indicate a block in the percolation pathway; therefore, the bond was labeled as "absent" otherwise it was "present." The pairwise comparison was repeated exhaustively for all bonds and plates. In the resulting lattice system, all the "absent" bonds were removed and the percolation network was formed by those "present" bonds only. The intersection criteria involve the transformation of the global coordinate system into a local system aligned with the elliptical surface. The same "binning" technique was applied here, i.e., the lattice system was divided into small domains encompassing the extreme locations of each elliptical plate, and only those bonds located inside the bin were examined for their relative positions. In this way, the computational effort associated with the pairwise comparisons was minimized.

### B. Percolation algorithm

For both ellipsoids and plates, the contact functions between the particles and the bonds/sites have been validated by graphically realizing the particles on computers followed by an inspection of their spatial locations relative to an arbitrary bond/site. A number of random realizations have been examined before the computational algorithms were implemented for the subsequent detection of percolation.

To find the percolation path in the resulting lattice network, a simulation scheme altered from the *burning algorithm*[22,23] was implemented. In particular, the sites or bonds located on an arbitrary side of the simulation domain were first identified. The connections between these sites/bonds and the adjacent ones in the system were then examined. For the site percolation system, each site had six neighboring sites, whereas for the bond percolation problem each bond had ten neighboring bonds. The connections were progressively examined and the process was repeated until no additional connections were found. When the process stopped, the system was detected as *percolated* if at least one site/bond on the opposite side of the simulation domain was found to be part of the interconnected

cluster. The process was intrinsically probabilistic for a finite system and the probability of percolation was determined as simply the ratio of the percolating cases to the total number of simulations performed. Since the probabilistic variation of the results depended on the particle size and number, an algorithm was developed to make the iteration process rather efficient. Specifically, the number of realization was variable depending on the particle diameter. This treatment was able to reduce the statistical variation in the simulation results thus improved the numerical accuracy. If the particle size approached zero, the result would be close to the threshold at which an infinite system percolates.

### C. Definitions of void percolation threshold

The percolation threshold of the ellipsoidal system can conveniently be defined as the volume fraction of the ellipsoids, or an invariant $\xi$ defined by

$$\xi = nV_0 = \frac{4}{3}n\pi r^2 t, \tag{3}$$

where $n$ is the particle density, i.e., the number of particles per unit volume, $V_0$ is the volume of a single ellipsoid, $r$ is the radius of revolution, $t$ is the half thickness, $r \geq t$. It should be pointed out that $\xi$ is related to the void volume fraction $f$ according to $f = e^{-\xi}$.

The definition of the percolation threshold for elliptical plates should be consistent with that of the equivalent three-dimensional systems rather than planar systems.[24] We define the following variable to measure the percolation threshold for thin elliptical plates:

$$\eta = \frac{4}{3}n\,\pi R^3 \tag{4}$$

and

$$A_0 = \pi R^2 = \pi ab, \tag{5}$$

where $R$ is the equivalent radius; $a$ and $b$ are the semi-axis lengths of ellipse; $n$ is the plate number per unit volume; $A_0$ is the area of a single ellipse. To make the simulation results comparable between ellipsoids and ellipses, especially in the limiting case when an oblate ellipsoid of revolution is reduced to a thin disk, an alternative definition of percolation threshold in terms of $\eta$ in Eq. (4) has been introduced for ellipsoids as well. Therefore, $\xi$ and $\eta$ are simply two different, but equivalent manners to define percolation threshold of ellipsoids. However, for ellipsoids, "$R$" should be interpreted as the radius of revolution "$r$" rather than the equivalent radius of ellipses defined in Eq. (5). Clearly, the relationship between $\xi$ and $\eta$ for oblate ellipsoids can be expressed as follows:

$$\eta = \varepsilon\xi = \frac{r}{t}\xi = \frac{R}{t}\xi. \tag{6}$$

Therefore, given one of the two thresholds, the other can be inferred readily.

## III. RESULTS

### A. Determination of void percolation thresholds

Figures 1 and 2 show the visualized computational models of oblate ellipsoids and elliptical plates, respectively. In each figure, one hundred equisized particles are generated on the computer forming an interconnected, random network inside a unit cell. These graphs are presented for visualization only, with the particle size being exaggerated and the particle numbers being much fewer than the actual numbers generated in the simulations. In real simulations, the radius of revolution ($r$) for ellipsoids and the equivalent radius ($R$) of ellipses were fixed to 0.015 and 0.03, respectively, in order to minimize the scaling effects. This resulted in a total particle number of 100 000–400 000 depending on the particle aspect ratio in each realization near the percolation threshold. The corresponding computational time was about 10–30 min for percolation detection in a single realization on a standard Intel Core Duo processor.

Apparently, the percolation probability is dependent on the particle density. To estimate the percolation threshold, the percolation probability was calculated with a subsequently increasing particle density from zero to a value significantly above the percolation point. The simulation was repeated fifty times in each case to compute the percolation probability for a specific total number of particles. The percolation threshold was then estimated from the particle density at a percolation probability of 50% by interpolation. Finally, this procedure was repeated for different pixel numbers $p$. In the current study, five different $p$'s: 300, 400, 500, 600, and 700 were chosen to estimate the percolation threshold by extrapolation, as illustrated in Fig. 3(a). The percolation value was plotted as a function of $p$ and the curve fitting technique was applied to obtain a parabola, whose constant term determines the percolation threshold when $p$ approaches infinity. Alternatively, the data can be fit to a power law
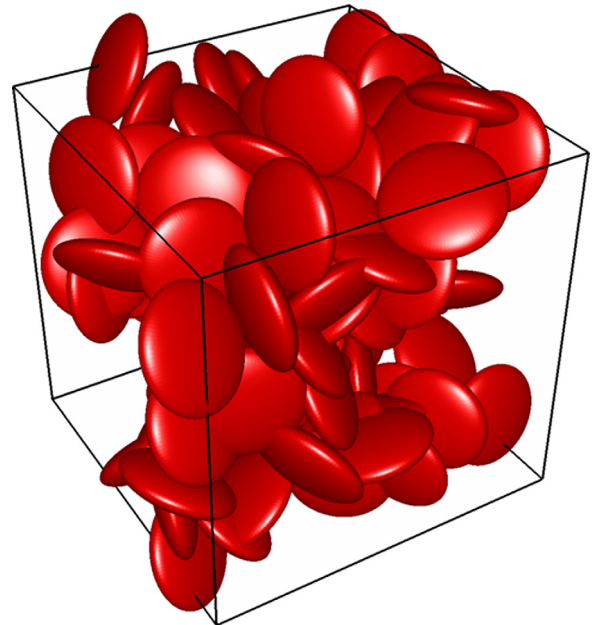


FIG. 1. Computer-generated 100 random oblate ellipsoids of aspect ratio 5.
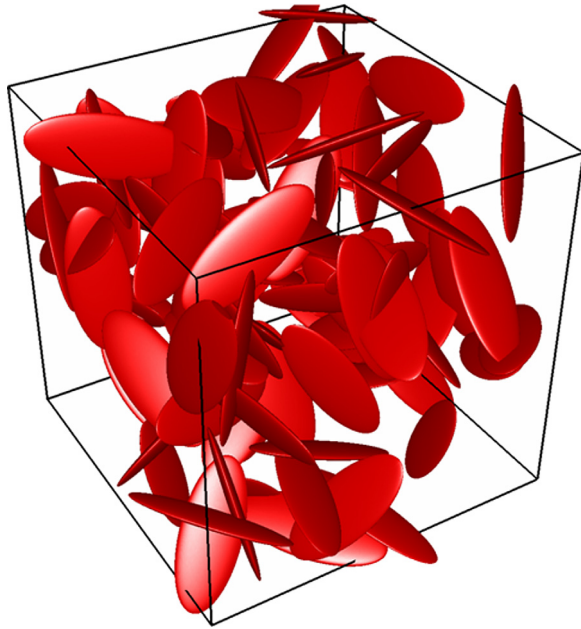
FIG. 2. Computer-generated 100 random elliptical thin plates of aspect ratio 3.
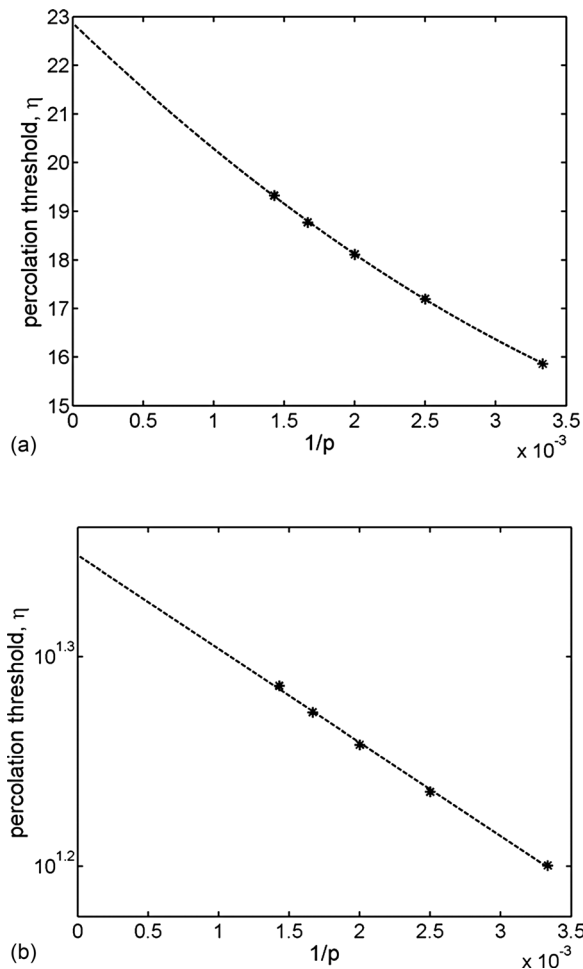


FIG. 3. Void percolation threshold of circular disks as a function of $1/p$ (where $p$ is the pixel number per side), determined from (a) parabolic curve fitting; (b) power law curving fitting.

function as shown in Fig. 3(b). In general, it has been found that a polynomial curving fitting consistently yields a better accuracy in terms of the norms of the residuals, and therefore, this method has been used in the current study. In fact, either a polynomial fit or a power law fit yields an almost linear relationship when $1/p$ approaches zero. Consequently, the results obtained from both curve fitting schemes do not differ much ($\eta = 22.86$ from the parabola versus $\eta = 22.30$ from the power law).

The procedure was then repeated for different aspect ratios to obtain the percolation threshold as a function of $\varepsilon$. A linear extrapolating function may also be applicable here but would reduce the numerical accuracy. The above values of pixel numbers were chosen due to the considerations on the computer memory and the processor speed.

### B. Void percolation thresholds of oblate ellipsoids

For oblate ellipsoids, the simulation results are presented in Figs. 4 and 5, and also tabulated in Table I along with the error estimation. The errors were estimated from the norms of the residuals via a standard error analysis of polynomial curve fit. It can be seen that the percolation threshold $\eta$ or $\xi$ changes with the aspect ratio $\varepsilon$. But the relationship is clearly nonlinear. When the ellipsoids degenerate to spheres, the result is $\eta = \xi = 3.515 \pm 0.006$. This is very close to the precise solutions reported in the literature[16,17] ($\eta = 3.503 \pm 0.010$). This result also converges to the limiting case for prolate particles reported previously.[18] When $\varepsilon$ increases to 10, $\xi$ becomes 1.542 and $\eta$ is 15.42. Because the equivalent radius is maintained constant, the new value of $\xi$ indicates that less than half of the particles are needed to reach void percolation in comparison with spheres. The relationship between the percolation threshold and aspect ratio was approximated in terms of polynomial functions. Although other forms of approximation, such as exponential function, logarithm functions, or power law functions are also possible, it is found that the polynomial fitting yields noticeably small standard deviations and therefore has been chosen to present the results in the current study. The dashed curves in Figs. 4 and 5 are fourth order polynomial
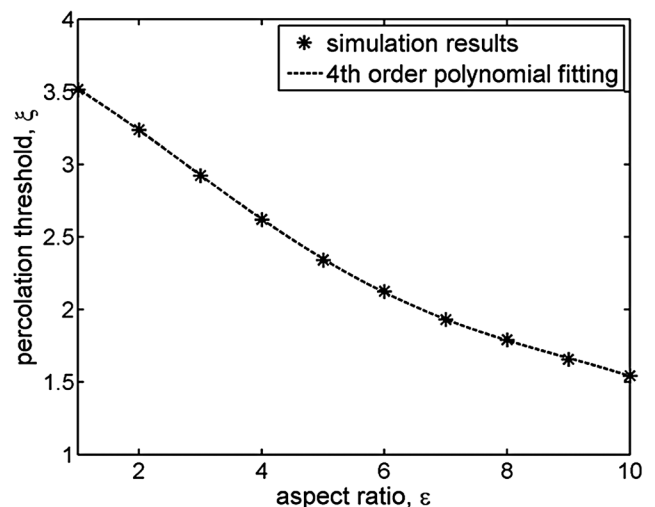


FIG. 4. Void percolation threshold, $\xi$, of oblate ellipsoids as a function of particle aspect ratio, $\varepsilon$.
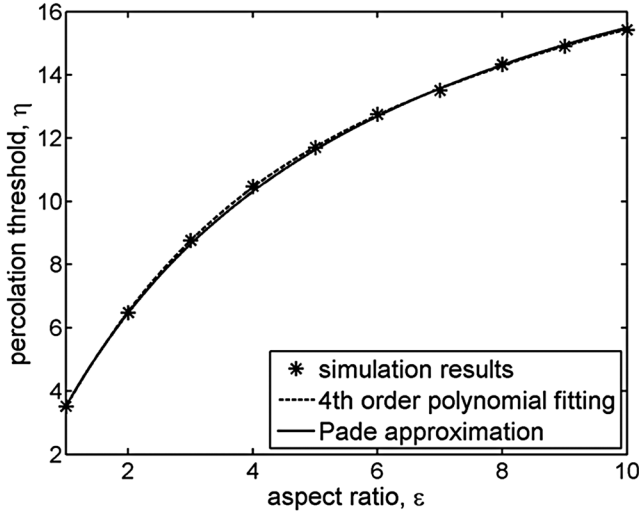
FIG. 5. Void percolation threshold, $\eta$, of oblate ellipsoids as a function of particle aspect ratio, $\varepsilon$.



FIG. 6. Void percolation threshold, $\eta$, of elliptical thin plates as a function of plate aspect ratio, $\varepsilon$.

approximations by curve fitting for ellipsoids, with the form of $\xi$ as follows:

$$\xi = -0.0004053\varepsilon^4 + 0.009462\varepsilon^3 - 0.05941\varepsilon^2 \\ - 0.16627\varepsilon + 3.7344; \ 1 \le \varepsilon \le 10 \qquad (7)$$

and $\eta$ as follows:

$$\eta = -0.001482\varepsilon^4 + 0.04828\varepsilon^3 - 0.6353\varepsilon^2 \\ + 4.601\varepsilon - 0.5102; \ 1 \le \varepsilon \le 10. \qquad (8)$$

In comparison with prolate ellipsoids, it has been noticed that the void percolation threshold of oblate particles has a much stronger dependence on the particle aspect ratio. For example, $\eta$ increases by more than three times when $\varepsilon$ increases from 1 to 8 for oblate ellipsoids. Meanwhile the same $\eta$ has changed by approximately 10% for prolate ellipsoids in the same situation.[18] Therefore, we need to pay special attention to the effects of aspect ratio on the void percolation of oblate particles.

Noted that Eqs. (7) and (8) are valid in the range of $\varepsilon$ between 1 and 10 only. It is clear, however, that $\eta$ will vary between the extreme values for oblate ellipsoids of $\varepsilon$ ranging between 10 and infinity. It has been found that a Pade approximant can cover the entire range of the aspect ratio and the result is following:

$$\eta = \frac{-0.7467 + 5.0357\varepsilon}{1 + 0.2203\varepsilon}; \ 1 \le \varepsilon \le \infty, \qquad (9)$$

where the three constants are determined from the data points at $\varepsilon = 1$, 2, and $\infty$. Note that the last data point can be

obtained from the circular plate problem. The result from this Pade approximation can be seen in Fig. 5.

## C. Void percolation thresholds of elliptical thin plates

For elliptical plates, the simulation results are presented in Fig. 6 and tabulated in Table II. They show that the percolation threshold increases with the aspect ratio, meanwhile it follows an approximately linear relationship with the aspect ratio for large values of $\varepsilon$. When the elliptical plates are reduced to circular disks, $\eta = 22.86$. As $\varepsilon$ increases to 10, $\eta$ becomes 57.34, which is 2.51 times greater than the threshold at $\varepsilon = 1$. These results have also been approximated as a fourth order polynomial by curve fitting with the following expression:

$$\eta = 0.004170\varepsilon^4 - 0.1108\varepsilon^3 + 1.020\varepsilon^2 \\ + 0.2861\varepsilon + 21.64; \ 1 \le \varepsilon \le 10. \qquad (10)$$

For an aspect ratio greater than 10, an approximate formula is presented here for providing an asymptotic limit:

$$\eta = 3.9080\varepsilon + 18.267; \ \varepsilon > 10. \qquad (11)$$

Thin disks can be considered as a degenerate geometry from oblate ellipsoids of zero thickness or infinite aspect ratio. Therefore, the percolation threshold in terms of $\eta$ for oblate ellipsoids of large aspect ratios should converge to the thin disks solution. From Fig. 5, it is seen $\eta = 15.42$ for $\varepsilon = 10$, which falls below the upper bound given by $\varepsilon = 1$, $\eta = 22.86$ in Fig. 6. When the aspect ratio of ellipsoids increases beyond 10, it is expected that $\eta$ will also increase according to the trend of $\eta$ shown in Fig. 5. In the limit, the

TABLE I. Void percolation thresholds of oblate ellipsoids.

| $\varepsilon$ | 1 | 2 | 3 | 4 | 5 | 6 | 7 | 8 | 9 | 10 |
|---|---|---|---|---|---|---|---|---|---|---|
| $\eta$ | $3.515 \pm 0.006$ | $6.478 \pm 0.008$ | $8.768 \pm 0.009$ | $10.47 \pm 0.02$ | $11.70 \pm 0.02$ | $12.75 \pm 0.04$ | $13.51 \pm 0.02$ | $14.33 \pm 0.02$ | $14.90 \pm 0.03$ | $15.42 \pm 0.01$ |
| $\xi$ | $3.515 \pm 0.006$ | $3.239 \pm 0.004$ | $2.923 \pm 0.003$ | $2.618 \pm 0.005$ | $2.340 \pm 0.004$ | $2.125 \pm 0.007$ | $1.930 \pm 0.003$ | $1.791 \pm 0.003$ | $1.656 \pm 0.003$ | $1.542 \pm 0.001$ |

TABLE II. Void percolation thresholds of elliptical thin plates.

| $\varepsilon$ | 1 | 2 | 3 | 4 | 5 | 6 | 7 | 8 | 9 | 10 |
|---|---|---|---|---|---|---|---|---|---|---|
| $\eta$ | $22.86 \pm 0.02$ | $25.37 \pm 0.01$ | $29.14 \pm 0.01$ | $32.94 \pm 0.02$ | $37.48 \pm 0.08$ | $41.43 \pm 0.06$ | $45.65 \pm 0.05$ | $49.47 \pm 0.07$ | $53.48 \pm 0.03$ | $57.34 \pm 0.05$ |

result will converge to the value of circular disks $\eta = 22.86$ as $\varepsilon$ approaches infinity. Therefore, Figs. 5 and 6 indeed demonstrate the connection between the circular disks and the ellipsoids in the limiting case.

These results for both oblate ellipsoids and elliptical plates indicate that not only the volume fractions but also the aspect ratio plays an important role in void percolation. It has been shown that it is generally not appropriate to treat the inclusions as either spheres or circular disks, even when the aspect ratio is not very far from unity. It should be pointed out that in the above simulations the minor axis of a particle should contain a reasonable number of sites/bonds to ensure the computational accuracy. Consequently, the major axis must not be too long. It has therefore imposed a restriction on the maximum aspect ratio that the current simulation technique is able to handle. This is the main reason that the particle aspect ratio discussed above was limited to those values below 10.

## IV. CONCLUSIONS

The void percolation thresholds were computed using a lattice mapping technique for both oblate ellipsoids and elliptical thin plates in three-dimensional space. The effects of the aspect ratio for some representative values between 1 and 10 were investigated in both cases. The results were expressed in the form of polynomial functions and Pade approximants. Agreements have been found between the computational results with those found the literature in several limiting cases. The results show that the aspect ratio must be taken into consideration for oblate particles in void percolation systems. Also the dependence of the void percolation threshold on the aspect ratio of oblate systems is much stronger than that of prolate systems previously investigated. These findings are useful in providing an insight to the material density or porosity needed to reach a void percolation in some important applications related to multiscale advanced materials. The same lattice mapping technique may also be applied to percolation problems with particulate inclusions of more general shapes. The physical properties such as the electrical and thermal conductivities in the void phase can generally be expressed in the power law forms, which are similar to those of other heterogeneous random materials. The determinations of the required parameters in the power law functions, however, require additional solution techniques, such as the finite element scheme or the variational theories.[25] This issue will be addressed in the authors' future studies.

[1]D. Stauffer and A. Aharony, *Introduction to Percolation Theory*, 2nd ed. (Taylor & Francis, Bristol, 1992).
[2]S. Mohanty and M. Sharma, Phys. Lett. A **154**, 475 (1991).
[3]Y. B. Yi and A. M. Sastry, Proc. R. Soc. London, Ser. A **460**, 2353 (2004).
[4]S. Torquato, *Random Heterogeneous Materials* (Springer-Verlag, Inc., New York, 2002).
[5]J. Quintanilla, S. Torquato, and R. M. Ziff, J. Phys. A **33**, L399 (2000).
[6]J. A. Quintanilla and R. M. Ziff, Phys. Rev. E **76**, 051115 (2007).
[7]J. Quintanilla and S. Torquato, Phys. Rev. E **54**, 5331 (1996).
[8]E. J. Garboczi, K. A. Snyder, J. F. Douglas, and M. F. Thorpe, Phys. Rev. E **52**, 819 (1995).
[9]X. F. Xu, J. Eng. Mech. **135**, 1180 (2009).
[10]A. Klemm, R. Kimmich, and M. Weber, Phys. Rev. E **63**, 041514 (2001).
[11]T. Navessin, S. Holdcroft, Q. P. Wang, D. T. Song, Z. S. Liu, M. Eikerling, J. Horsfall, K. V. Lovell, J. Electroanal. Chem. **567**, 111 (2004).
[12]Y. B. Yi, H. Wang, A. M. Sastry, and C. M. Lastoskie, Phys. Rev. E **72**, 021913 (2005).
[13]P. V. K. Pant and R. H. Boyd, Macromolecules **26**, 679 (1993).
[14]R. Metzler and J. Klafter, Phys. Rep., Phys. Lett. **339**, 1 (2000).
[15]A. R. Kerstein, J. Phys. A **16**, 3071 (1983).
[16]M. D. Rintoul, Phys. Rev. E **62**, 68 (2000).
[17]C. D. Lorenz and R. M. Ziff, J. Chem. Phys. **114**, 3659 (2001).
[18]Y. B. Yi, Phys. Rev. E **74**, 031112 (2006).
[19]J. Sun and H. Weinstein, J. Chem. Phys. **127**, 155105 (2007).
[20]I. L. Novak, P. Kraikivski, and B. M. Slepchenko, Biophys. J. **97**, 758 (2009).
[21]J. W. Perram and M. S. Wertheim, J. Comput. Phys. **58**, 409 (1985).
[22]D. Dhar, Phys. Rev. Lett. **64**, 1613 (1990).
[23]P. Bak and K. Chen, Physica D **38**, 5 (1989).
[24]Y. B. Yi and E. Tawerghi, Phys. Rev. E **79**, 041134 (2009).
[25]X. F. Xu, Acta Mech. **223**, 765 (2012).